Mechanisms of Ageing and Development 180 (2019) 97–106

Contents lists available at ScienceDirect

Mechanisms of Ageing and Development

journal homepage: www.elsevier.com/locate/mechagedev

Oxidative stress-induced senescence markedly increases disc cell bioenergetics

Prashanti Patil[a,e], Micol Falabella[c,e], Amal Saeed[c,e], Dayeong Lee[a,e], Brett Kaufman[c,e], Sruti Shiva[d,e], Claudette St Croix[e,g], Ben Van Houten[e,f], Laura J. Niedernhofer[e,h], Paul D. Robbins[e,h], Joon Lee[a,e], Sowa Gwendolyn[a,b,e], Nam V. Vo[a,e,*]

[a] Department of Orthopedic Surgery, University of Pittsburgh, 200 Lothrop Street, Pittsburgh, PA, 15213, USA
[b] Department of Physical Medicine and Rehabilitation, University of Pittsburgh, 200 Lothrop Street, Pittsburgh, PA, 15213, USA
[c] Division of Cardiology, Vascular Medicine Institute, Department of Medicine, University of Pittsburgh School of Medicine, Pittsburgh, PA, 15213, USA
[d] Department of Pharmacology & Chemical Biology, University of Pittsburgh, Pittsburgh, PA 15261, USA
[e] Vascular Medicine Institute, University of Pittsburgh, Pittsburgh, PA, 15213, USA
[f] Department of Pharmacology and Chemical Biology, University of Pittsburgh Cancer Institute, Hillman Cancer Research Pavilion, Pittsburgh, PA, 15213, USA
[g] Center for Biological Imaging, Department of Cell Biology and Physiology, University of Pittsburgh, Pittsburgh, PA, 15219, USA
[h] Institute on the Biology of Aging and Metabolism, Department of Biochemistry, Molecular Biology and Biophysics, University of Minnesota, Minneapolis, MN, 55455 USA

ARTICLE INFO

Keywords:
Aging
Cellular senescence
Intervertebral disc degeneration
Matrix homeostasis
Bioenergetics
Mitochondria

ABSTRACT

Cellular senescence is a phenotype characterized by irreversible growth arrest, chronic elevated secretion of proinflammatory cytokines and matrix proteases, a phenomenon known as senescence-associated secretory phenotype (SASP). Biomarkers of cellular senescence have been shown to increase with age and degeneration of human disc tissue. Senescent disc cells in culture recapitulate features associated with age-related disc degeneration, including increased secretion of proinflammatory cytokines, matrix proteases, and fragmentation of matrix proteins. However, little is known of the metabolic changes that underlie the senescent phenotype of disc cells. To assess the metabolic changes, we performed a bioenergetic analysis of *in vitro* oxidative stress-induced senescent (SIS) human disc cells. SIS disc cells acquire SASP and exhibit significantly elevated mitochondrial content and mitochondrial ATP-linked respiration. The metabolic changes appear to be driven by the upregulated protein secretion in SIS cells as abrogation of protein synthesis using cycloheximide decreased mitochondrial ATP-linked respiration. Taken together, the results of the study suggest that the increased energy generation state supports the secretion of senescent associated proteins in SIS disc cells.

1. Introduction

Intervertebral disc degeneration (IDD) is one of the most common underlying causes of low back pain and disability in older adults (The Burden of Musculoskeletal Diseases in the United States (BMUS, 2008). The intervertebral disc tissue undergoes several structural, biochemical, and biomechanical changes with age, which ultimately impede the normal disc function and patient mobility. With increasing age, the disc tissue experiences loss and fragmentation of matrix proteins, specifically aggrecan, the major proteoglycan (PG), with concomitant decrease in water content, leading to fissures and decreased disc height (Roughley, 2004). Multiple reports suggest that the elevated inflammatory cytokines, such as IL-6, IL-8, TNFα, and IL-1β, are closely associated with the development of IDD. These cytokines suppress synthesis of matrix proteins and upregulate secretion of matrix proteases that includes ADAMTS (A Disintegrin and Metalloproteinase with Thrombospondin motifs) -4 and -5, and MMP (matrix metalloproteinases)-1, -2, -3, -13, and -14 (Risbud and Shapiro, 2014). The age-related imbalance in matrix homeostasis of disc tissue suggests that the disc cells undergo phenotypic alteration. Indeed, the tissue milieu of the aged disc contains elevated quantities of inflammatory proteins and oxidants, two well-known inducers of cellular senescence. Thus, the age-related degeneration of disc tissue could be speculated to be driven by transformation of the disc cells into a senescenct phenotype.

Cellular senescence is functionally defined as the irreversible loss of cellular proliferative potential and can be induced by a wide array of stressors, which commonly involve DNA damage (Campisi, 2005). Historically, senescence was first characterized as the finite

* Corresponding author at: E1643 Biomedical Science Tower, 00 Lothrop Street, Pittsburgh, PA, 15213, USA.
E-mail address: von@upmc.edu (N.V. Vo).

https://doi.org/10.1016/j.mad.2019.04.006
Received 4 October 2018; Received in revised form 22 March 2019; Accepted 15 April 2019
Available online 17 April 2019
0047-6374/

proliferative capacity of primary human cells in culture, triggered by erosion in telomere length (Hayflick, 1965). Telomere attrition is found to generate persistent DNA damage response (DDR), which is needed to enforce the permanent growth arrest attained by serial cell passaging (d'Adda di Fagagna, 2008). In addition to the passage-dependent telomere shortening, other stressors are known to induce senescence as well. The best studied examples come from conditions in which cells are exposed to subtoxic doses of genotoxic stress that directly damage DNA (hydrogen peroxide, UV), termed stress-induced senescence (SIS). Senescence can also occur when cells experience strong and continuous mitogenic signals, termed oncogene-induced senescence (OIS) (Marazita et al., 2016; Serrano et al., 1997). Both SIS and OIS share several features with replicative senescence, including characteristic morphological changes, persistent DDR, irreversible growth arrest, and enhanced senescence-associated beta-galactosidase (SA-βGal) activity.

Growing evidence supports cellular senescence as one of the major drivers of aging and age-associated diseases (Childs et al., 2015). Indeed, senescent cells have been documented to increase with age in many rodent, non-human primate, and human tissues (Melk et al., 2004; Herbig, 2006; Wang et al., 2009). Moreover, an elevated number of senescent cells have been identified at the sites of several degenerative age-associated pathologies including osteoarthritis, glomerulosclerosis, and atherosclerosis (Campisi, 2011). Genetic or pharmacologic depletion of senescent cells in natural and progeroid mice, ameliorates age-related degenerative changes in several tissues and attenuates functional decline of skeletal and cardiac tissue (Baker et al., 2011; Baker et al., 2016; Zhu et al., 2015; Wang, 2015; Burton and Stolzing, 2018). The increase in the fraction of senescent cells has also been documented in degenerative and aging human discs (Le Maitre et al., 2007; Gruber et al., 2009). Recently, we reported a dramatic upregulation of $p16^{Ink4a}$, a cell cycle arrest protein that is known to be upregulated in senescent cells, and the accelerated loss of disc PG in mice chronically exposed to genotoxic stress, including tobacco smoke and ionizing radiation (Nasto et al., 2013). All together these studies suggest a correlative relationship between DNA damage-induced senescent cells and IDD.

While senescent cells' growth is arrested, they are far from inert. One of the most defining features of SIS and OIS cells is the elevated and chronic secretion of myriad inflammatory cytokines and matrix proteases. This robust secretory phenotype of senescent cells is termed as senescent-associated secretory phenotype (SASP) (Coppé et al., 2010). It is postulated that the senescent cells drive tissue aging through the action of SASP factors. *In vitro* and mouse xenograft studies have shown that the SASP factors can promote profound degenerative changes that ultimately compromise the tissue structure and function (Coppé, 2008). Furthermore, it was reported that the level of SASP factors provide predictive power regarding onset of disability and mortality in the elderly (Ferrucci et al., 1999; Alley et al., 2007). The bioenergetic demands of such robust SASP production is becoming an important area of aging research (Wiley, 2016).

Relatively little is known regarding the metabolic alterations that occur with cell entry into senescence. In RAS-induced and replication-induced senescent human fibroblast cells, impaired mitochondrial function and increased oxidant formation have been documented (Passos et al., 2007; Moiseeva et al., 2009). However, in oncogenic $BRAF^{V600E}$-induced senescence, metabolic rewiring to increase mitochondrial respiration was necessary to maintain growth arrest and elevated secretion of IL-6 and IL-8 SASP factors (Kaplon et al., 2013). Similarly, in chemotherapy-induced senescence, metabolic shift to elevated mitochondrial energy generation was needed to sustain the synthesis of NF-κB-mediated SASP factors (Dörr et al., 2013). These findings suggest that the elevated and chronic production of the proteins, including SASP factors, caused by multiple stressors drives increased energy production in senescent cells. However, none of the studies to date have elucidated whether such metabolic changes occur in the context of oxidative stress-induced senescent disc cells.

Table 1
Surgical patient information.

NP tissue ID	Age	Sex	Level of Degeneration	Diagnosis (eg. Cervical stenosis)
201623	33	M	2	Cervical Disc Displacement
201612	35	F	2	Cervical Disc Displacement
201830	36	F	3	Cervical Radiculopathy
201617	37	F	3	Cervical Stenosis
201622	39	F	2	Disc Herniation
201643	41	F	2	Cervical Spondylotic Radiculopathy
201624	46	M	3	Cervical Stenosis
201827	46	M	1	Cervical Radiculopathy
201611	47	F	2	Cervical Stenosis
201755	47	F	2	Cervical Stenosis
201642	50	F	3	Disc Herniation
201636	51	M	2	Cervical Stenosis
201710	51	F	2	Cervical Stenosis
201627	52	F	2	Cervical Stenosis
201632	53	F	2	Cervical Stenosis
201817	53	M	3	Cervical Radiculopathy
201631	56	M	3	Cervical Stenosis
201657	57	F	2	Disc Herniation
201820	58	M	3	Displacement of cervical intervertebral disc with radiculopathy
201736	74	M	4	Cervical Stenosis

Herein, we performed bioenergetic analysis of hydrogen peroxide-induced senescent human disc cells. In these SIS cells, we observed increased mitochondrial number, protein expression, and mitochondrial-ATP linked respiration, together with elevated fragmentation of matrix proteins and pro-inflammatory cytokines. Furthermore, protein synthesis in senescent disc cells was found to be supported by the increased mitochondrial respiration. Our findings suggest that SIS disc cells acquire enhanced bioenergetics to support secretion of senescence-associated proteins.

2. Methods

2.1. Samples collection and cell isolation

Human nucleus pulposus disc samples were obtained from surgical specimens from patients aged 50 ± 11.4 years (mean ± SD) with mean degeneration grade of 2.41 ± 0.5 on the Thompson grading scale (IRB #: PRO12100603) (See Table 1). Cells were isolated from digested tissues as previously described (Vo et al., 2013). Cells were cultured in monolayer in F-12 media (Cat. No. 11765-062, *Life Technologies)* under low oxygen conditions (37 °C, 5% CO2, and 5% O2 with a bicarbonate buffer to maintain pH 7.2).

2.2. Senescence induction

Hydrogen peroxide was used to induce cellular senescence as previously described (Ngo et al., 2017). Briefly, primary human nucleus pulposus (hNP) cells were treated with 500 μM hydrogen peroxide in F-12 (Cat. No. 11765-062, *Life Technologies),* supplemented with 10% Fetal Bovine Serum (FBS; Cat. No. S12450, *Atlanta Biologicals*;) and 1% Penicillin/Streptomycin solution (PS; Cat. No. 15140-16, *Life Technologies*), for 2 h. Culture media was then replaced with fresh F-12 with 10% FBS and 1% PS media without hydrogen peroxide. Cells were then maintained in culture for 10 days to establish senescence.

2.3. Senescence-associated β-galactosidase staining

Senescence-associated β-galactosidase (SA β-gal) staining was performed as previously described (Dimri et al., 1995). Images were taken using brightfield microscopy at 10X magnification.

2.4. ELISA

Conditioned media was collected at the end of culture (day 10) and concentrated 40x with 3 kDa cutoff centrifugal concentrators (Cat. No. UFC 900324, *Millipore Sigma*). IL-6 and IL-8 protein levels were determined using *R&D Total Human IL6 and IL8 DuoSets* (Cat. No. DY206 and DY208, respectively). Level of CTX-II, a degradative fragment derived from the C terminus of collagen type II, was measured using *Biomatik Cross Linked C-Telopeptide of Type II Collagen kit* (Cat. No. EKU03505) as per manufacturer's instruction. Protein concentration was normalized to cell number assessed by tryphan blue exclusion.

2.5. Immunoblotting

To assess aggrecan fragmentation, conditioned media was collected at day 10 of culture and concentrated as described above. To assess p53 protein expression levels, protein extracts from cell cultures were obtained using *T-PER Tissue Protein Extraction Reagent* supplemented with proteinase inhibitor cocktail as per the manufacturer's instructions (Cat. No. 78510, *Thermo Fisher*). Concentrated conditioned supernatant and cell lysates from cell cultures were separated using Tris-HEPES 4–20% gradient polyacrylamide denaturing gel (Cat. No. 25204, *Thermo Scientific*). The amount of conditioned media and cell lysates loaded on the gel corresponded to equal cell number. After electrophoresis, the proteins were transferred to a PVDF membrane by electroblotting and processed as described before (Ngo et al., 2017). Immunoreactive proteins were detected using chemiluminescent detection system (Cat. No. 34096, *Thermo Scientific* and Bio-Rad *ChemiDoc MP*). The following primary and secondary antibodies were used: Aggrecan (Cat.No. ab36861 (anti-G1), *Abcam*), p53 (Cat.No. 2524, *CST*) and β-actin (Cat.No. PA1-183, *Thermo Fisher*), anti-rabbit goat secondary antibody with HRP (Cat. No. PI-31460, *Thermo Scientific*). Quantification was performed with densitometry analysis using *Bio-Rad* ChemiDoc MP.

2.6. Bioenergetic flux measurement by Seahorse XFe96

Bioenergetic measurements were performed using Seahorse Extracellular Flux Analyzer. The protocol for adherent cells was adapted to disc cells (Qian, 2010). Briefly, hydrogen peroxide-treated and untreated disc cells were plated at a density of 80,000 cells per well on a XFe96 plate and cultured overnight in F-12 media (10% FBS and 1% P/S). On the day of the experiment, cell culture media was replaced with unbuffered DMEM (Cat. No. D5030, *Sigma Aldrich*) supplemented with 2 mM Glutamax-1 (Cat. No. A1286001, *Gibco*), 1 mM sodium pyruvate (Cat. No. P5280, *Sigma*), 25 mM glucose (Cat. No. G7021, *Sigma*), 32 mM sodium chloride (Cat. No. S3014, *Sigma Aldrich*), and 15 mg phenol red (Cat. No. P3532, *Sigma Aldrich*) and incubated in non-CO2 incubator at 37 °C. Extracellular flux measurements were performed three times at six-minute intervals over five different treatment conditions: basal, oligomycin (2.5 μM) (Cat. No. 75351, *Sigma*), carbonyl cyanide-*4*- (trifluoromethoxy) phenylhydrazone (FCCP) (2.5 μM) (Cat. No. C2920, *Sigma Aldrich*), 2-deoxglucose (2DG) (100 mM) (Cat. No. D6134, *Sigma Aldrich*), and rotenone (Cat. No R-8875, *Sigma Aldrich*) and antimycin A (Cat. No. A8674, *Sigma*) (2 μM each). Oxygen consumption rate (OCR) and extracellular acidification rate (ECAR) were calculated at each measurement. OCR and ECAR calculations were normalized by cell number per well using the tryphan blue exclusion assay. Mitochondrial ATP-linked respiration was calculated by subtracting the OCR values after oligomycin addition from the Basal OCR values. The proton leak was calculated by subtracting the OCR values after rotenone and antimycin A addition from basal OCR values.

To assess the relationship between protein production and upregulation of bioenergetic parameters, 2.5 μg/ml cycloheximide (CHX), an inhibitor of protein synthesis, was added to hydrogen peroxide-treated and untreated cells for 24 h before measuring extracellular flux parameters.

2.7. Immunofluorescent staining

Cells were washed twice with cold PBS and fixed in 2% paraformaldehyde in PBS for 15 min at room temperature. Cells were then permeabilized with 0.25% Triton X-100, and blocked with 20% serum (using the species in which the secondary antibodies were made) and 1% BSA in PBS (PBB) for 45 min at room temperature. Cells were incubated with the specific primary antibodies for γH2AX (Cat. No. 05-636, *Millipore*), mtDNA (Cat. No. 03-61014, *American Research Products, Inc.*), TOM20 (Cat. No.PA5-52843, *ThermoFisher Scientific*) or ATP synthase beta (Cat. No. A-21351, *ThermoFisher Scientific*) overnight at 4 °C. Cells were then washed three times with PBB and incubated with secondary antibody. The following secondary antibodies were used: 488 anti-rabbit (Cat. No. A21206, *Life Technologies*), Cy3 AffiniPure Goat anti-mouse (Cat. No. 115-165-003, *JacksonImmuno Research*) or Alexa Fluor 647 AffiniPure Goat anti-rabbit (Cat. No. 111-605-003, *Jackson Immuno Research*) for 1 h at room temperature. To assess mtDNA colocalization with mitochondria, Cy3 (mtDNA) and Hoechst (BIsbenzimide; Cat. No. B-2883, *Sigma-Aldrich*) were collected simultaneously and Cy5 (TOM20) was collected by sequential scanning frames using a Leica TCS SP8 system. The images were then deconvolved through Huygens Professional software (SVI). Images of cells stained with anti γH2AX antibodies were acquired with an Eclipse TE2000-U (*Nikon*, Minato, Tokyo, JP).

2.8. Mitochondrial quantification

To assess mitochondrial morphology, we performed immunofluorescent analysis of fixed cells using TOM20 (Cat. No.PA5-52843, *ThermoFisher Scientific*) to label mitochondria. Cells were co-stained with Hoechst (nuclei). Confocal Z-stacks were collected using a 60X (1.43NA) optic on a Nikon A1 equipped with GASP detectors and NIS Elements software (*Nikon Inc.*, Melville NY). The confocal datasets were imported into Imaris (Bitplane Zurich, Switzerland) for surface rendering and calculation of mitochondrial number, volume, and sphericity.

2.9. mtDNA measurements

Total DNA from primary human nucleus pulposus (hNP) cells was isolated by sodium dodecyl sulfate lysis and proteinase K digestion as previously described (Kolesar et al., 2013). DNA was then resuspended at 37 °C in Tris-EDTA buffer containing RNAse A and the total DNA concentration determined by fluorescence using AccuBlue Broad range kit (Biotium, Fremont, CA). mtDNA and nDNA abundance was measured by duplex qPCR using three different TAQMAN primer/probes sets (ND1 and B2M; CytB and GUSB; Cox1 and ACTB) and averaged. Serial dilutions of combined samples were also performed to confirm assay linearity and dilution independence of results. qPCR was conducted on a StepOnePlus thermo cycler (ThermoFisher Scientific) using TaqMan Fast Advanced Master Mix (ThermoFisher Scientific), 4.6 ng/reaction DNA, and 5 μM of primer/probes in 10 μl final reaction volume. Relative mtDNA abundance was calculated by the ΔΔCq method (Livak, 2001). The qPCR amplification profile was: one cycle (95 °C for 20 s) and 40 cycles (95 °C for 1 s and 60 °C for 20 s). Assays for mtDNA (mtND1, mtCYTB, and mtCOXI) were primer limited (1 primer: 1 probe), whereas assays for nuclear DNA (B2M, GUSB, ACTB) were not primer limited (3 primer: 1 probe). The primers and probes used for the mtDNA quatification were purchased from Integrated DNA Technologies (IDT) and are listed below (Table 2).

2.10. Transmission Electron Microscopy (TEM) imaging

SIS and non-SIS disc cells were fixed in cold 2.5% glutaraldehyde in 0.01 M PBS for 1 h at room temperature. The specimens were rinsed in PBS, treated with 1% osmium tetroxide/1% potassium ferricyanide,

Table 2
Primers used for qPCR for mtDNA measurements.

mtND1 probe	5'-/5HEX/CCATCACCC/ZEN/TCTACATCACCGCCC-3'
mtND1 primer 1	5'-GAGCGATGGTGAGAGCTAAGGT-3'
mtND1 primer 2	5'-CCCTAAAACCCGCCACATCT-3'
B2M probe	5'-/6FAM/ ATGTGTCTG/ZEN/GGTTTCATCCATCCGACA -3'
B2M primer 1	5'- TCTCTCTCCATTCTTCAGTAAGTCAACT-3'
B2M primer 2	5'- CCAGCAGAGAATGGAAAGTCAA-3'
mtCYTB probe	5'-/5HEX/ATCATCCGC/ZEN/TACCTTCACGCCAAT-3'
mtCYTB primer 1	5'-CCACATCACTCGAGACGTAAAT -3'
mtCYTB primer 2	5'-GATGTGTAGGAAGAGGCAGATAAA -3'
GUSB probe	5'-/6FAM/AAGAGTGGT/ZEN/GCTGAGGATTGGCA-3'
GUSB primer 1	5'-TGGTACGAACGGGAGGT -3'
GUSB primer 2	5'-ACGATGGCATAGGAATGGG -3'
mtCOXI probe	5'-/5HEX/TGCCATAAC/ZEN/CCAATACCAAACGCC-3'
mtCOXI primer 1	5'-CTAGCAGGTGTCTCCTCTATCT -3'
mtCOXI primer 2	5'-GAGAAGTAGGACTGCTGTGATTAG-3'
ACTB probe	5'-/6FAM/CTGCCTCCA/ZEN/CCCACTCCCA-3'
ACTB primer 1	5'-GTCCCCCAACTTGAGATGTATG-3'
ACTB primer 2	5'-AAGTCAGTGTACAGGTAAGCC -3'

rinsed in PBS, dehydrated through a graded series of ethanol and propylene oxide, and then embedded in Poly/Bed® 812 (Luft formulations). Semi-thin (300 nm) sections were cut on a Leica Reichart Ultracut, stained with 0.5% Toluidine Blue in 1% sodium borate and examined under the light microscope. Ultrathin sections (65 nm) were stained with uranyl acetate and Reynold's lead citrate and examined on JEOL 1011 transmission electron microscope with a side mount AMT 2k digital camera (Advanced Microscopy Techniques, Danvers, MA).

2.11. Protein synthesis

Disc cells were cultured for 24 h in F-12 media containing 10% FBS and 1% PS in a 6-well plate in the presence of 10 μCi/ml 3H-*L*-proline at 37 °C. The cells were either supplemented with 2.5, 5, 10 μg/ml cycloheximide (CHX) or left untreated (0 μg/ml CHX) at the start of the assay. The conditioned media (CM) was collected and the cell samples suspended in homogenizing buffer (20 mM Tris-HCl, 200 mM NaCl, 100 mM glycine, 0.1% Triton × 100, 50 μM DTT, 0.1 mg/ml soybean trypsin inhibitor) and subjected to three freeze/thaw cycles at the end of the 24 h incubation period. The samples were then stirred at 4 °C for overnight, the CM and cell layer combined, and protein synthesis determined by 3H-proline incorporation using a previously established method (Gilberston et al., 2008).

2.12. Cell viability

The quantity of disc cells in presence of 0, 2.5, 5, and 10 μg/ml cycloheximide (CHX) was determined using Picogreen assay kit (Cat. No. P7589, *ThermoFisher Scientific*) as before (Gilberston et al., 2008).

2.13. General statistical analysis

Shapiro-Wilk test was used to test for normality. Student independent *t*-test was used to analyze data found to be normal. For two variable non-parametric data, the Mann-Whitney test was used. Analysis of variance (ANOVA) with Bonferroni correction for multiple comparison was used in cases of data with multi-variables. Statistics were derived using GraphPad Prism from GraphPad Software (San Diego, CA). All graphs show mean values with error bars (SD or SEM, as defined in the figure legends), unless specified otherwise. $P < 0.05$was considered significant.

3. Results

3.1. Establishment of oxidative stress induced senescent disc culture system

To better understand the phenotype of cellular senescence and its role in driving disc tissue aging, it would be ideal to isolate and characterize the native senescent cells from disc tissue. However, this is technically challenging as no single specific biomarker of senescent cells, and disc senescent cells in particular, has been identified to allow for selection and isolation. Therefore, we made use of a previously engineered *in vitro* model to induce senescence in human disc cells derived from surgical specimens using hydrogen peroxide (H_2O_2) (Ngo et al., 2017). The rationale for this experimental approach was twofold: 1) H_2O_2 induces oxidative damage, an established feature in aged disc tissue; 2) H_2O_2 provokes DNA damage, a well-known hallmark of cellular senescence (Rodier et al., 2009). hNP cells were treated with hydrogen peroxide to induce DNA damage and incubated in culture media sans hydrogen peroxide for 10 days to allow cells to establish stress-induced senescence (SIS). This treatment regime ensured that the observed changes were in fact due to senescent phenotype and not to H_2O_2-induced transient oxidative stress experienced by cells. To confirm establishment of the senescent phenotype, we assessed the expression of γH2AX, p53, and senescence-associated beta galactosidase (SA-βgal) activity (Fig. 1A–C). Senescent cells are typically characterized by DNA damage response, cell growth arrest, and increased activity of the lysosomal hydrolase β-galactosidase (SA-βgal) (Bernadotte et al., 2016). γH2AX, a H2AX histone phosphorylated at the C-terminal serine-139, is a sensitive marker of DNA damage, particularly double-stranded DNA breaks. p53 is a transcription factor that induces the expression of p21, an inhibitor of the cyclin dependent kinases, leading to G1 arrest (Rufini et al., 2013). Hence, increased expression of p53, increased γ-H2AX foci, and increased SA-βgal activity indicate cellular senescence. At 10 days post-H_2O_2 treatment, 90% of the hNP cells expressed p53 protein and contained nuclear foci of γH2AX. In addition, most of the cells stained positive for SA-βgal and displayed a flattened and enlarged cell morphology that is commonly associated with senescent phenotype in these cells. Detection of these markers confirmed successful induction and establishment of SIS disc cells. It should also be noted that although different NP cells from different donors exhibited some phenotypic variations, they all showed a consistent senescent phenotype by expressing these senescent markers.

3.2. Senescent disc cells acquire a catabolic phenotype that is reminiscent of an older disc tissue phenotype

To test for markers of age-related IDD, we assessed matrix catabolism in SIS disc cells. The aggrecan fragmentation mediated by ADAMTS and MMP class of proteases was 30x and 5x higher in SIS compared to non-SIS disc cells, respectively (Fig. 2A). The level of collagen II fragmentation, assayed by measuring CTX-II ELISA (Charni-Ben Tabassi et al., 2008) in hNP SIS cells, was modestly, but not significantly, increased as well (Fig. 2B). We next tested levels of proinflammatory cytokines, including IL-6 and IL-8, which are known to promote the increased collagen and aggrecan fragmentation with age by inducing synthesis of MMP and ADAMTS class of proteases in disc cells. Indeed, we observed greater than 10x increase in lL-6 and IL-8 protein levels in media from hNP SIS cultures compared to that of non-SIS cells (Fig. 2C). This suggested that SIS disc cells, by virtue of their elevated secretion of proinflammatory cytokines (IL-6 and IL-8), can promote MMP and ADAMTS catalyzed matrix protein fragmentation seen with aging in disc tissue.

3.3. Mitochondrial respiration is increased in stress-induced senescent disc cells

One key feature of senescent cells is their elevated and chronic

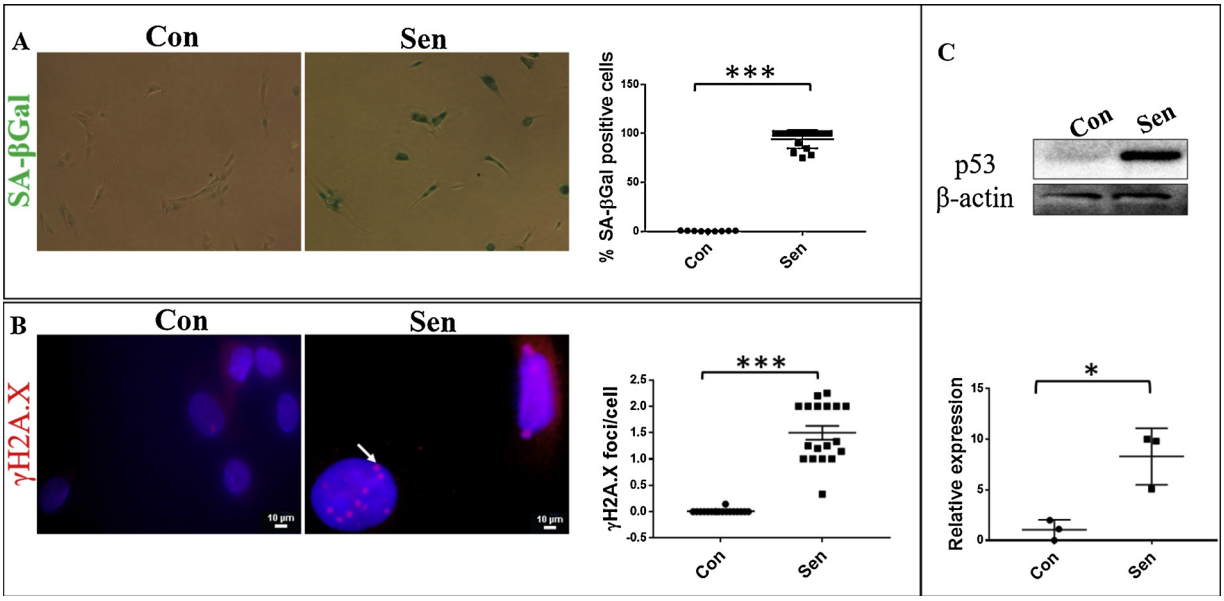

Fig. 1. *Establishment of stress-induced senescence (SIS) in disc cells:* Senescence phenotype establishment in human disc cells treated with hydrogen peroxide (500 μM, 2 h and examined 10 days later) was verified by SA-βGal staining (A), punctated expression of the DNA damage response marker γH2AX in nuclei (B), and p53 protein expression (C). The individual points in (A) indicate the percent SA- βGal positive cells in one field of imaging and in (B) indicate the number of γH2AX foci divided by the number of cells (DAPI) in one field of imaging. Data in (A) and (B) are means ± SEM of 4 independent experiments. The graphs in (C) indicate volume of p53 band divided by volume of β-actin band from 3 independent experiments. Data in (C) is means ± SD; ***p < 0.0001; *p < 0.05. Scale bar = 10μM.

secretion of numerous proteins, including pro-inflammatory cytokines and matrix proteases. We hypothesized that increased chronic protein secretion is an energetically demanding process, and we therefore examined the bioenergetic profile of SIS disc cells using Seahorse Flux Analyzer, which measures cellular glycolytic and oxidative phosphorylation (OXPHOS) rates simultaneously. The glycolysis activity is measured via changes in the extracellular acidification rate (ECAR) and OXPHOS activity is assessed via oxygen consumption rate (Fig. 3A, B). The SIS disc cells had a significantly higher (182%) basal OCR compared to non-SIS disc cells (Fig. 3C). The SIS disc cells also had higher ECAR, though not statistically significant, than that of the non-SIS disc cells. Since the increase in basal OCR could be driven by either increase in mitochondrial ATP-linked respiration or proton leak, we examined the sensitivity of the cells to oligomycin, an inhibitor of ATP synthase (complex V) and to rotenone and antimycin A compounds, which inhibit complex I and III, respectively (Mito ATP and Proton leak OCR, described in Fig. 3). The mitochondrial respiration associated with ATP production was significantly higher (165%) in SIS cells compared to non-SIS disc cells. However, the mitochondrial respiration associated with proton leak did not change appreciably, suggesting the increase in basal OCR is driven by increased mitochondrial ATP-linked respiration (Fig. 3C).

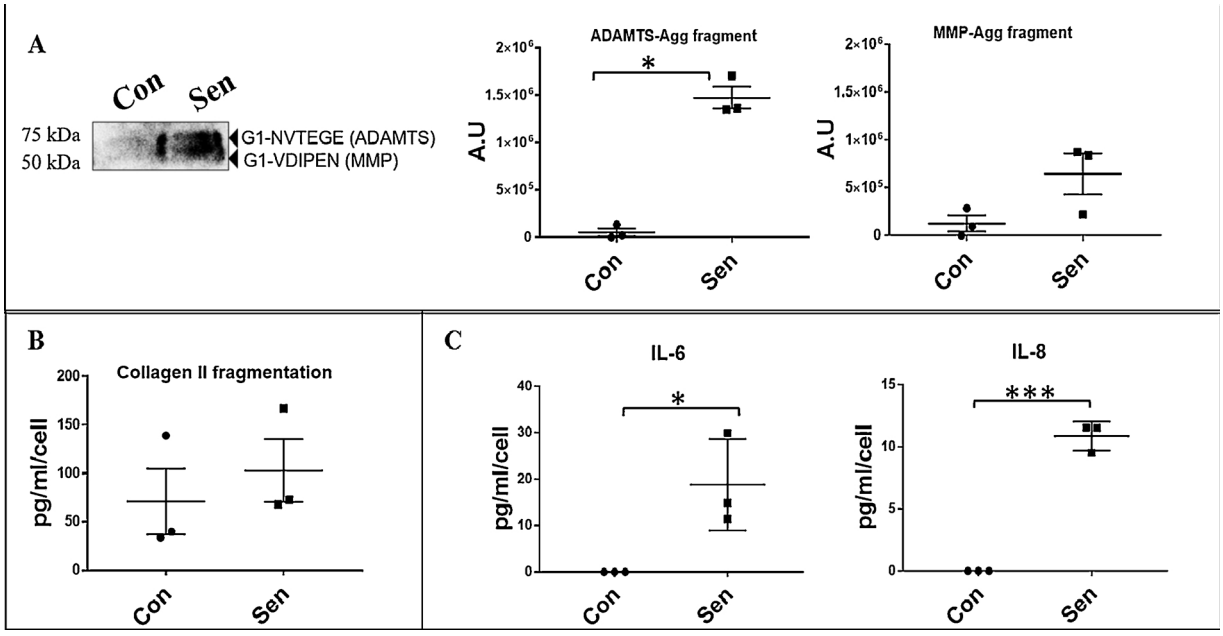

Fig. 2. *SIS disc cells mirror markers of age-related disc degeneration:* SIS disc cells display elevated levels of aggrecan fragments mediated by action of ADAMTS and MMP proteases as assessed by Western blot (A), collagen II fragments (B), and IL-6 and IL-8 proteins by ELISA (C). Data are means ± SD of 3 independent experiments; ***p < 0.0001; *p < 0.05.

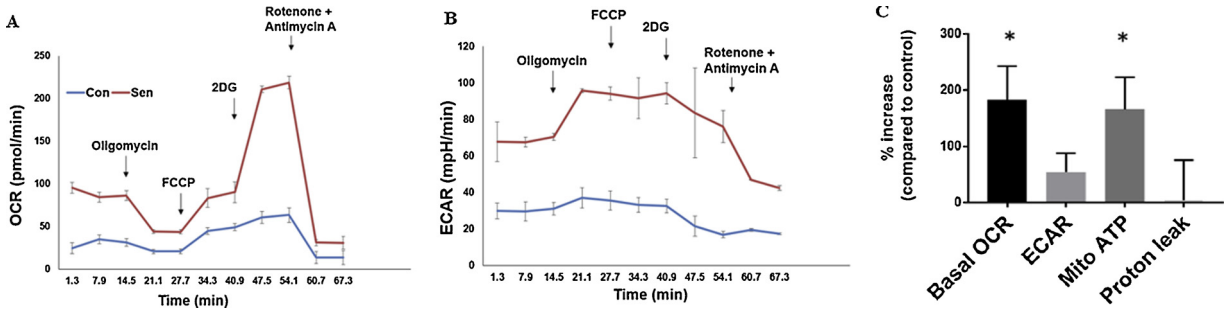

Fig. 3. *SIS disc cells exhibit alteration in energy metabolism*: 80×10^3 SIS and non-SIS disc cells were plated in Seahorse XF96 Extracellular Flux Analyzer plate. The Seahorse Analyzer records rates of OXPHOS and glycolysis via the oxygen consumption rate (OCR) and the extracellular acidification rate (ECAR). Basal OCR and ECAR are recorded at the start of the assay and the metabolic inhibitors (oligomycin, carbonyl cyanide 4- (trifluoromethoxy) phenylhydrazone (FCCP), 2-deoxyglucose (2DG), and rotenone and antimycin A) were added sequentially to distinguish cellular reliance upon glycolysis and oxidative phosphorylation. The plots in A and B illustrate OCR and ECAR trace of a single seahorse experiment. Each dot in A and B represent a time at which OCR or ECAR was measured. A) Basal OCR is calculated from the mean time points of 1-3. ATP- linked OCR (Mito ATP) is calculated by taking the basal OCR and subtracting the mean of time points 4 and 5 (oligomycin). Proton leak is calculated by taking the mean of time points 4 and 5 and subtracting the mean of time points 10 and 11 (rotenone and antimycin A). B) Glycolytic activity is assessed by recording the extracellular acidification rate (ECAR). Basal ECAR is calculated from the mean of time points 1-3. C) Plot illustrates increased basal and ATP-linked respiration in senescent (Sen) compared to non-senescent (Con) disc cells. Error bars in A and B represent standard deviation of the mean. The data in C is representative of 5 independent experiments and expressed as means ± SEM; *p < 0.05.

3.4. Increased mitochondrial content accompanies the increased mitochondrial respiration in senescent disc cells

Increase in mitochondrial ATP-linked respiration is typically driven by increased mitochondrial biogenesis. First, we assessed mitochondrial protein expression by 2D imaging SIS and non-SIS disc cells labeled with antibodies against ATP synthase beta and TOM20. ATP synthase beta is a mitochondria specific protein that is integral to the electron transport chain complex V. TOM20 is a mitochondrial membrane protein that helps in translocating cytosolically synthesized proteins destined for mitochondria. The expression of both these mitochondrial proteins was higher in SIS compared to non-SIS disc cells (Fig. 4A, B). Next, we assessed mitochondrial number and morphology by 3D imaging SIS and non-SIS disc cells labeled with TOM20. The data sets from the imaging were imported into Imaris software for surface volume rendering using intensity based segmentation to identify discrete objects (mitochondria). The SIS disc cells had significantly more objects compared to non-SIS disc cells, suggesting a greater number of discrete mitochondrial units (Fig. 4C). As the volume per mitochondrial unit was similar, the difference is most likely explained by increased mitochondrial abundance rather than increased fission, which would be expected to be associated with increased fragmentation and decreased volume per fragment (Fig. 4E). There were no differences in the shape/morphology of the individual mitochondria as reflected by sphericity (roundness) measurements (Fig. 4D). The sphericity parameter is defined as the ratio of the surface area of the given object to the surface area of a sphere with the same volume as the given object; the closer the sphericity value is to 1, the more spherical the object. Consistently,

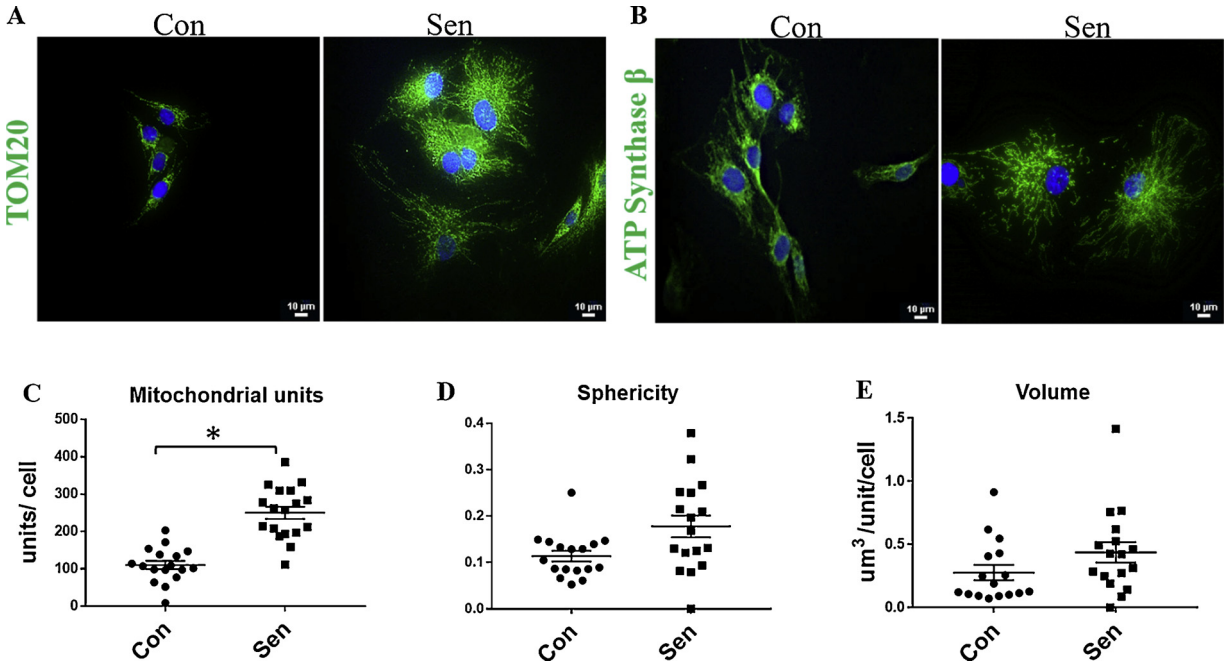

Fig. 4. *SIS disc cells have increased mitochondrial content compared to non-SIS disc cells:* Expression of TOM20 (A) and ATP synthase beta (B) in SIS and non-SIS disc cells as assessed by immunofluorescence imaging. To assess mitochondrial number and morphology, 3D imaging of SIS and non-SIS disc cells labelled with anti-TOM20 antibody was carried out. The data sets from imaging were imported into Imaris software for surface rendering. The 3-D surface rendering revealed higher number of mitochondria in SIS disc cells (C) but similar sphericity (D) and volume (E). The individual data points in C and E represent the number of surface unit or volume divided by the number of cells (DAPI) in one field of imaging. Data are means ± SEM of 3 independent experiments; *p < 0.05. Scale bar = 10μM.

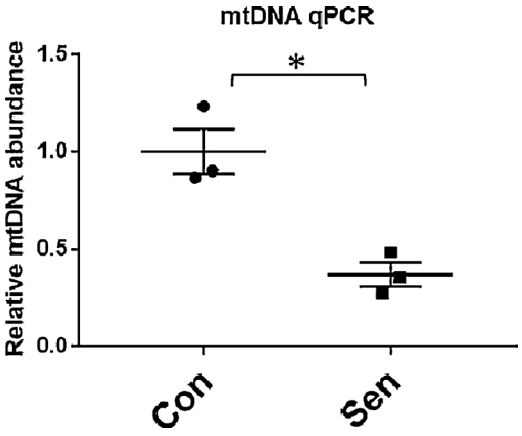

Fig. 5. *SIS disc cells have lower mtDNA compared to non-SIS disc cells:* The relative mtDNA levels in the population was determined by averaging the results of three quantitative PCR assays after normalization to nuclear DNA. SIS disc cells contained significantly lower amounts of mtDNA relative to non-SIS disc cells. Data are means ± SD of 3 independent experiments; *p < 0.05.

morphological assessment done using EM imaging of SIS and non-SIS disc cells revealed similarity in terms of mitochondrial cristae and membrane structure between SIS and non-SIS disc cells (Sup 2).

Next, we examined the levels of mtDNA by quantitative PCR in SIS and non-SIS disc cells (Fig. 5). To ensure against sequence variation, we used three mtDNA/nDNA multiplex TAQMAN primer/probe sets. Unexpectedly, the qPCR results revealed the SIS disc cells to contain ˜37% of the mtDNA levels of non-SIS disc cells (Fig. 5). Thus, the increase in mitochondria respiration in SIS disc cells occurs without the expected increase in mtDNA content. Additionally, we performed immunohistochemistry for mtDNA levels in both cell types (Fig. 6) and found altered in situ levels and distribution of mtDNA in SIS disc cells. Specifically, while most mtDNA localized with TOM20 in non-SIS disc cells, much of mtDNA did not localize with TOM20 in SIS disc cells. Hence, SIS disc cells not only contain lower quantity of mtDNA, but much of their mtDNA is cytoplasmic, i.e., not residing within the mitochondria.

3.5. *The elevated mitochondrial respiration in senescent disc cells is driven by the increased protein synthesis*

To determine whether the increased mitochondrial ATP-linked respiration was in fact needed for the elevated production of the proteins, we assessed the mitochondrial bioenergetics profile of SIS and non-SIS disc cells in presence of the protein synthesis inhibitor cycloheximide (CHX). Consistent with our earlier observation, SIS disc cells had significantly increased basal OCR rate compared to non-SIS disc cells (Fig. 7A). However, upon treatment with CHX, the SIS disc cells had 7x lower basal OCR rate compared to untreated SIS disc cells. The basal OCR difference between CHX treated and untreated non-SIS disc cells was very minimal. The reduction in basal OCR rate in SIS disc cells treated with CHX was found to be primarily driven by lower mitochondrial respiration needed for ATP production as the oligomycin sensitive respiration in SIS disc cells treated with CHX was significantly lower compared to untreated SIS disc cells (Fig. 7B); no such appreciable difference in proton leak between SIS cells treated with CHX compared to untreated SIS cells was found (Fig. 7C). The ATP-linked respiration and proton leak difference in CHX treated and untreated non-SIS disc cells was very modest. These results collectively suggested that the high mitochondrial ATP-linked respiration in SIS disc cells is needed in synthesis of proteins, presumably to maintain SASP where an abundance of inflammatory and catabolic factors is produced and secreted.

4. Discussion

Senescent cells accumulate in multiple tissues with age in vertebrate organisms and contribute to the decline in tissue homeostasis via secretion of myriad catabolic factors that can have potent impact on neighboring cells and surrounding tissues. Multiple reports have shown an increase in cellular senescence with age and degeneration in human and rodent discs (Le Maitre et al., 2007; Gruber et al., 2007; Nasto et al., 2013). The relationship between cellular senescence and age-related disc degeneration may be more than correlative, as work done by Ngo et al. (2017) has shown that human senescent disc cells express elevated amounts of matrix proteases as well as proinflammatory cytokines, factors that are known to promote loss of disc tissue health with aging. However, no study to date has explored the underlying metabolic changes of senescent disc cells.

In the present study, we demonstrated elevated production of the key SASP factors IL-6 and IL-8, which mirror the increased aggrecan fragmentation in SIS disc cells. We also discovered that SIS disc cells harbor a substantially greater number of mitochondria and exhibit increased mitochondrial ATP-linked respiration. We speculate that this metabolic alteration of increased mitochondria ATP-linked respiration

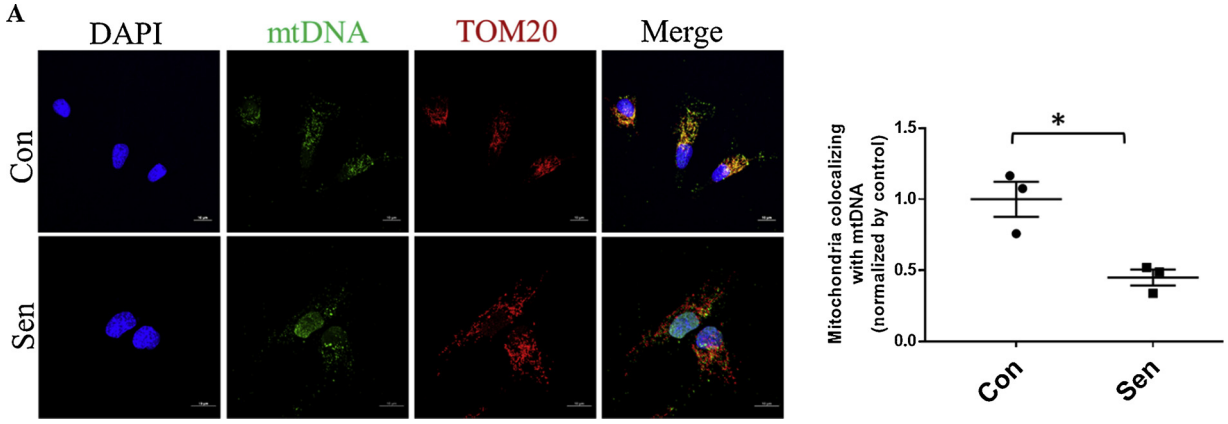

Fig. 6. *The SIS disc cells mtDNA do not localize with mitochondria:* mtDNA (green) and mitochondria (red) were detected in situ by immunohistochemistry in SIS and non-SIS disc cells by fluorescent microscopy (see methods). To quantify mtDNA resident in mitochondria, images were deconvolved and fluorescence volume of mtDNA that co-localized with mitochondria was divided by the total fluorescence volume of mtDNA for each sample. The average of three samples were calculated for each group and normalized to control values (100%). Similar results were achieved with object counting instead of volume determination (data not shown). The graph on right is the quantification of results from three independent experiments. Data is expressed as means ± SD; *p < 0.05 (For interpretation of the references to colour in this figure legend, the reader is referred to the web version of this article).

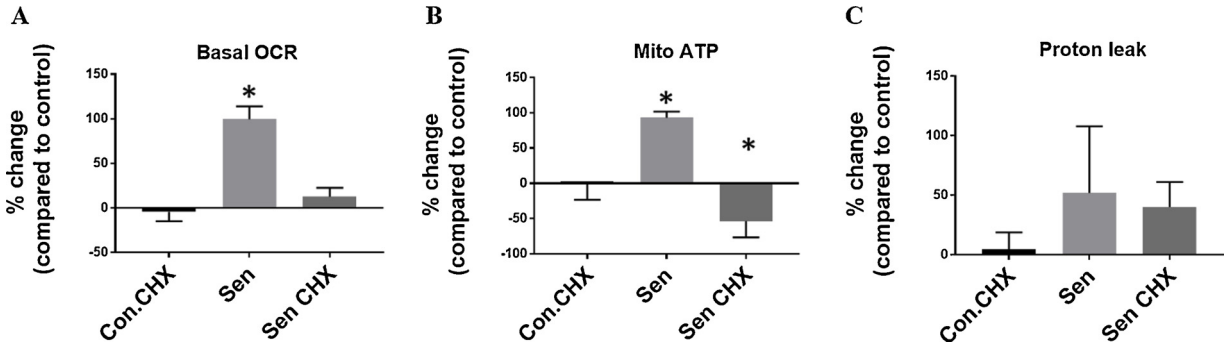

Fig. 7. *Suppression of protein synthesis dampens mitochondrial-ATP linked OCR in SIS disc cells:* 80×10^3 SIS and non-SIS disc cells were plated in a well of Seahorse XF96 Extracellular Flux Analyzer and incubated with or without 2.5 μg/ml of cycloheximide (CHX) for 24 h before commencing Seahorse recording of the basal OCR and ECAR and OCR after addition of sequential addition of metabolic inhibitors. A) The high basal OCR in SIS disc cells is abrogated after inhibition of protein synthesis using CHX. Assessment of mitochondrial-ATP linked OCR (Mito ATP) (B) and proton leak OCR (C) in presence of CHX suggests that the reduction in basal OCR in SIS cells in A is due to dampening of mitochondrial ATP- linked respiration and not due to proton leak. Data are means ± SEM of 4 independent experiments; *$p < 0.05$.

in disc cells is necessary to meet the energy demand elicited by the elevated production of proteins in senescent cells. This idea is supported by our experiment showing that inhibition of protein synthesis significantly lowered mitochondrial ATP-linked respiration in SIS but not control disc cells. Our finding is also consistent with other reported studies which show that in chemotherapy and oncogene-induced senescent cells, lower macromolecule synthesis (fatty acids) and high mitochondrial ATP production are metabolic adaptations necessary to maintain the persistent and high protein production, including SASP factors (Dörr et al., 2013; Quijano et al., 2012).

The mitochondria's role in cellular senescence has been widely associated with generation of ROS, which acts as a driver of signaling networks necessary to maintain the senescent phenotype (Passos et al., 2010). However, recent work has shed light on the true necessity of mitochondria for senescence in addition to ROS generation. Report by Correia-Melo et al. (2016) demonstrated that in irradiation-induced senescent fibroblasts, suppression of a vast number of genes involved in senescence was seen upon depletion of mitochondria by treatment with CCCP, an uncoupler that targets the ubiquitin ligase Parkin to mitochondria and promotes their degradation. In accordance with this, the protein synthesis in SIS disc cells was seen to drive the elevated mitochondrial ATP-linked respiration. This result was unexpected as disc cells are known to rely on glycolysis for generation of ATP. Therefore, it can be derived that the disc cells upon becoming senescent become adapted to generate energy via OXPHOS to support synthesis of senescent related peptides.

Increased mitochondrial number and protein expression were found to be the changes accompanying the upregulation in mitochondrial ATP-linked respiration in SIS disc cells. However, surprisingly, no concurrent increase in mtDNA levels was seen in SIS disc cells. The conundrum of increased mitochondrial function with lower mtDNA is not unprecedented, however. Heddi *et al.* observed coordinated increase in nuclear and mitochondrial OXPHOS transcripts in muscle of MERRF (myoclonic epilepsy associated with red ragged fibers) and MELAS (myopathy, encephalopathy, lactic acidosis, and stroke-like episodes) patients with diagnosed mutation in mitochondrial genome (Heddi et al., 1993). Work by Piechota *et al.* showed that in HeLa cells, despite a reduction in mtDNA by 90%, the COX2 protein and COX activity were 6-fold higher relative to mtDNA content. Taken together, these results suggest that the depletion in mtDNA can be compensated by increased transcription per genome and efficient protein synthesis (Piechota et al., 2006). Interestingly, the mtDNA in SIS disc cells did not co-localize with mitochondria and was mostly cytoplasmic. Cytoplasmic DNA is a known trigger for the cytosolic DNA sensor cGAS to produce second messenger cyclic GMP-AMP (cGAMP), which binds and activates the adaptor protein STING, thereby leading to the production of inflammatory cytokines. The cGAS-STING pathway plays an essential role in restraining microbial infection. Recently, it was shown that cGAS-STING also helps in initiation and maintenance of SASP factors in cells induced to senescence by various means (Dou et al., 2017; Yang et al., 2017; Gluck et al., 2017). It therefore is possible that cytoplasmic mtDNA of SIS disc cells plays a role in regulating the SASP factor synthesis. However, this remains to be verified.

Alteration in metabolic state of cells is accompanied by changes in mitochondrial morphology. Specifically, mitochondrial fusion is favored under energetically demanding conditions as it allows for complementation of genes and efficient dissipation of membrane potential (Westermann B, 2012). Mitochondrial fission, on the other hand, helps maintain bioenergetic state of the cell by promoting degradation of damaged organelle by autophagy (Westermann, 2012). The mitochondria in SIS disc cells had similar cristae structure, outer membrane definition, sphericity, and volume compared to non-SIS disc cells. In contrast, previous reports show that in human cell lines induced to undergo senescence there is an overall shift to more fusion events, resulting in abnormally elongated mitochondria (Lee et al., 2007; Park et al., 2010). However, it is unclear if elongated mitochondria are truly needed to maintain permanent growth arrest in all cell types or whether such morphological changes are only seen in transformed cell lines.

Despite the morphological similarity between SIS and non-SIS disc cell mitochondria, mitochondrial ATP-linked respiration in senescent disc cells is elevated. It cannot be discounted that this upregulation in SIS disc cells, which would consequently lead to higher mitochondrial ATP concentration, could be utilized towards processes other than protein synthesis. In chemotherapy-induced senescent cells, part of the mitochondrial ATP-linked respiration was shown to be devoted to autophagic degradation of the improperly synthesized and processed senescent-associated secretory peptides (Dörr et al., 2013). It was speculated that the increased secretion of the catabolic factors by senescent cells overwhelms the cells capacity for proper protein synthesis, post-translation modification, vesicular transport, and secretion. Hence, it is plausible that in SIS disc cells the mitochondrial ATP-linked respiration could be utilized by mechanisms which alleviate the proteotoxic stress. Nevertheless, protein synthesis is positioned at the top of the hierarchy of ATP-consuming processes in cells (Buttgereit and Brand, 1995). Therefore, in senescent disc cells most of the mitochondrial ATP-linked respiration is probably utilized by protein synthesis. Whether the SASP proteins (IL-6 and IL-8) in senescent disc cells specifically induce the upregulation in ATP-linked respiration remains to be tested. Previous published reports have shown that pro-inflammatory cytokines positively facilitate increased energy generation in different human cell types in vitro and in tissues in vivo (Tan et al., 2018). Hence it is possible that the pro-inflammatory cytokines

produced by senescent disc cells could upregulate energy production in these cells. In summary, the results of this study collectively suggest that the SIS disc cells attain a catabolic phenotype and display marked upregulation in mitochondrial ATP-linked respiration to support protein synthesis.

Funding sources

The work was supported by the National Institute of Health (AG044376 to NV, GM110424 to BAK and MF, AG043376 and AG056278 to PDR and LJN, and 1S10RR019003-01 Shared Instrument Grant). We would like to acknowledge the NIH supported microscopy resources in the Center for Biologic Imaging. Specifically the confocal microscope supported by grant number 1S10OD019973-01.

Conflict of interest

LJN is a SAB member of Innate Biologics and Castle Creek; PDR is a SAB member of Innate Biologics, Tissuegene, Unicyte and co-founder of Genascence.

Acknowledgements

We would like to thank Catherine Corey for help with running the Seahorse extracellular flux assays and Jessa Darwin for editorial support.

Appendix A. Supplementary data

Supplementary material related to this article can be found, in the online version, at doi:https://doi.org/10.1016/j.mad.2019.04.006.

References

Alley, D.E., Crimmins, E., Bandeen-Roche, K., Guralnik, J., Ferrucci, L., 2007. Three-year change in inflammatory markers in elderly people and mortality: the Invecchiare in Chianti study. J. Am. Geriatr. Soc. 55, 1801–1807.

Baker, D., Childs, B., Durik, M., Wijers, M., Sieben, C., Zhong, J., Deursen, J., 2011. Clearance of p16Ink4a- positive senescent cells delays ageing-associated disorders. Nature 479, 232–236.

Baker, D.J., Childs, B.G., Durik, M., Wijers, M.E., Sieben, C.J., Zhong, J., Saltness, R.A., Jeganathan, K.B., Verzosa, G.C., Pezeshki, A., Khazaie, K., Miller, J.D., van Deursen, J.M., 2016. Naturally occurring p16(Ink4a)-positive cells shorten healthy lifespan. Nature 530 (Feb. (7589)), 184–189. https://doi.org/10.1038/nature16932. Epub 2016 Feb 3.

Bernadotte, A., Mikhelson, V., Spivak, I., 2016. Markers of cellular senescence. Telomere shortening as a marker of cellular senescence. Aging (Albany NY) 8 (1), 3–11.

Burton, D.G.A., Stolzing, A., 2018. Cellular senescence: immunosurveillance and future immunotherapy. Ageing Res. Rev. 43, 17–25.

Buttgereit, F., Brand, M., 1995. A hierarchy of ATP-consuming processes in mammalian cells. Biochem. J. 312 (1), 163–167.

Campisi, J., 2005. Senescent cells, tumor suppression, and organismal aging: good citizens, bad neighbors. Cell 120 (5), 513–522.

Campisi, J., 2011. Cellular senescence: putting the paradoxes in perspective. Curr. Opin. Genet. Dev. 21 (1), 107–112.

Charni-Ben Tabassi, N., Desmarais, S., Bay-Jensen, A.C., Delaissé, J.M., Percival, M.D., Garnero, P., 2008. The type II collagen fragments Helix-II and CTX-II reveal different enzymatic pathways of human cartilage collagen degradation. Osteoarthr. Cartil. 16 (10), 1183–1191.

Childs, B., Durik, M., Baker, D., van Deursen, J., 2015. Cellular senescence in aging and age-related disease: from mechanisms to therapy. Nat. Med. 21 (12), 1424–1435.

Coppé, J., Patil, C., Rodier, F., Sun, Y., Muñoz, D., Goldstein, J., Campisi, J., 2008. Senescence associated secretory phenotypes reveal cell-nonautonomous functions of oncogenic RAS and the p53 tumor suppressor. PLoS Biol. 6 (12), e301.

Coppé, J., Desprez, P., Krtolica, A., Campisi, J., 2010. The senescence-associated secretory phenotype: the dark side of tumor suppression. Annu. Rev. Pathol. 5, 99–118.

Correia-Melo, C., Marques, F., Anderson, R., Hewitt, G., Hewitt, R., Cole, J., Passos, J., 2016. EMBO J. 35 (7), 724–742.

d'Adda di Fagagna, F., 2008. Living on a break: cellular senescence as a DNA-damage response. Nat. Rev. Cancer 8, 512–522.

Dimri, G.P., Lee, X., Basile, G., Acosta, M., Scott, G., Roskelley, C., Medrano, E.E., Linskens, M., Rubelj, I., Pereira-Smith, O., et al., 1995. A biomarker that identifies senescent human cells in culture and in aging skin in vivo. Proc. Natl. Acad. Sci. USA 92 (20), 9363–9367.

Dörr, J., Yu, Y., Milanovic, M., Beuster, G., Zasada, C., Däbritz, J., Schmitt, C., 2013. Synthetic lethal metabolic targeting of cellular senescence in cancer therapy. Nature 501 (7467), 421–425.

Dou, Z., Ghosh, K., Vizioli, M.G., Zhu, J., Sen, P., Wangensteen, K.J., Berger, S.L., 2017. Cytoplasmic chromatin triggers inflammation in senescence and cancer. Nature 550 (7676), 402–406.

Ferrucci, L., Harris, T., Guralnik, J., Tracy, R., Corti, M., Cohen, H., Havlik, R., 1999. Serum IL-6 level and the development of disability in older persons. J. Am. Geriatr. Soc. 47, 639–646.

Gilberston, L., Ahn, S.-H., Teng, P.-N., STuder, R., Niyibizi, C., Kang, J., 2008. The effects of rhBMP-2, rhBMP-12, and Ad-BMP-12 on matrix synthesis in human annulus fibrosus and nucleus pulposus cells. Spine J. 8 (3), 449–456.

Gluck, S., Guey, B., Gulen, M.F., Wolter, K., Kang, T.W., Schmacke, N.A., Ablasser, A., 2017. Innate immune sensing of cytosolic chromatin fragments through cGAS promotes senescence. Nat. Cell Biol. 19 (9), 1061–1070.

Gruber, H.E., Ingram, J.A., Norton, H.J., Hanley, E.N., 2007. Senescence in cells of the aging and degenerating. Intervertebral Disc. SPINE. 32 (3), 321–327.

Gruber, H., Ingram, J., Davis, D., Hanley, E., 2009. Increased cell senescence is associated with decreased cell proliferation in vivo in the degenerating human annulus. Spine J. 9, 210–215.

Hayflick, L., 1965. Limited in vitro lifetime of human diploid cell strains. Exp. Cell Res. 37, 614–636.

Heddi, A., Lestienne, P., Wallace, D.C., Stepien, G., 1993. Mitochondrial DNA expression in mitochondrial myopathies and coordinated expression of nuclear genes involved in ATP production. J. Biol. Chem. 268 (16), 12156–12163.

Herbig, U., 2006. Cellular senescence in aging Primates. Science 311 (5765) 1257–1257.

Kaplon, J., Zheng, L., Meissl, K., Chaneton, B., Selivanov, V., Mackay, G., Peeper, D., 2013. A key role for mitochondrial gatekeeper pyruvate dehydrogenase in oncogene-induced senescence. Nature 498, 109–112.

Kolesar, J., Wang, C., Taguchi, Y., Chou, S., Kaufman, B., 2013. Two-dimensional intact mitochondrial DNA agarose electrophoresis reveals the structural complexity of the mammalian mitochondrial genome. Nucleic Acids Res. 41 e58-e58.

Le Maitre, C., Freemont, A., Hoyland, J., 2007. Accelerated cellular senescence in degenerate intervertebral discs: a possible role in the pathogenesis of intervertebral disc degeneration. Arthritis Res. Ther. 9, 45.

Lee, S., Jeong, S.Y., Lim, W.C., Kim, S., Park, Y.Y., Sun, X., Youle, R.J., Cho, H., 2007. Mitochondrial fission and fusion mediators, hFis1 and OPA1, modulate cellular senescence. J. Biol. Chem. 282, 22977–22983.

Livak, K., Schmittgen, T., 2001. Analysis of relative gene expression data using real-time quantitative PCR and the 2(-Delta Delta C(T)) Method. Methods 25, 402–408.

Marazita, M., Dugour, A., Marquioni-Ramella, M., Figueroa, J.A., 2016. Oxidative stress-induced premature senescence dysregulates VEGF and CFH expression in retinal pigment epithelial cells: implications for age-related macular degeneration. Redox Biol. 7, 78–87.

Melk, A., Schmidt, B., Takeuchi, O., Sawitzki, B., Rayner, D., Halloran, P., 2004. Expression of p16INK4a and other cell cycle regulator and senescence associated genes in aging human kidney. Kidney Int. 65 (2), 510–520.

Moiseeva, O., Bourdeau, V., Roux, A., Deschênes-Simard, X., Ferbeyre, G., 2009. Mitochondrial dysfunction contributes to oncogene-induced senescence. Mol. Cell. Biol. 29, 4495–4507.

Nasto, L., Wang, D., Robinson, A., Clauson, C., Ngo, K., Dong, Q., Vo, N., 2013. Genotoxic stress accelerates age-associated degenerative changes in intervertebral discs. Mech. Ageing Dev. 134 (1–2), 35–42.

Ngo, K., Patil, P., McGowan, J., Niedernhofer, L., Robbins, P., Kang, J., Vo, N., 2017. Senescent intervertebral disc cells exhibit perturbed matrix homeostasis phenotype. Mech. Ageing Dev. 166, 16–23.

Park, Y.Y., Lee, S., Karbowski, M., Neutzner, A., Youle, R.J., Cho, H., 2010. Loss of MARCH5 mitochondrial E3 ubiquitin ligase induces cellular senescence through dynamin-related protein 1 and mitofusin 1. J. Cell. Sci. 123, 619–626.

Passos, J., Saretzki, G., Ahmed, S., Nelson, G., Richter, T., Peters, H., von Zglinicki, 2007. Mitochondrial dysfunction accounts for the stochastic heterogeneity in telomere-dependent senescence. PLoS Biol. 5 (5), 110.

Passos, J.F., Nelson, G., Wang, C., Richter, T., Simillion, C., Proctor, C.J., Miwa, S., Olijslagers, S., Hallinan, J., Wipat, A., Saretzki, G., Rudolph, K.L., Kirkwood, T.B.L., von Zglinicki, T., 2010. Feedback between p21 and reactive oxygen production is necessary for cell senescence. Mol. Syst. Biol. 6 (347).

Piechota, J., Szczesny, R., Wolanin, K., Chlebowski, A., Bartnik, E., 2006. Nuclear and mitochondrial genome responses in HeLa cells treated with inhibitors of mitochondrial DNA expression. Acta Biochim. Pol. 53 (3), 485–495.

Qian, W., Van Houten, B., 2010. Alterations in bioenergetics due to changes in mitochondrial DNA copy number. Methods 51 (4), 452–457.

Quijano, C., Cao, L., Fergusson, M., Romero, H., Liu, J., Gutkind, S., Finkel, T., 2012. Oncogene induced senescence results in marker metabolic and bioenergetic alterations. Cell Cycle 11 (7), 1383–1392.

Risbud, M.V., Shapiro, I.M., 2014. Role of cytokines in intervertebral disc degeneration: pain and disc content. Nat. Rev. Rheumatol. 10 (1), 44–56.

Rodier, F., Coppé, J.P., Patil, C.K., Hoeijmakers, W.A., Muñoz, D.P., Raza, S.R., Campisi, J., 2009. Persistent DNA damage signalling triggers senescence-associated inflammatory cytokine secretion. Nat. Cell Biol. 11, 973–979.

Roughley, P.J., 2004. Biology of intervertebral disc aging and degeneration: involvement of the extracellular matrix. Spine 29 (23), 2691–2699.

Rufini, A., Tucci, P., Celardo, I., Melino, G., 2013. Senescence and aging: the critical roles of p53. Oncogene 32 (43), 5129–5143.

Serrano, M., Lin, A.W., McCurrach, M.E., Beach, D., Lowe, S.W., 1997. Oncogenic ras provokes premature cell senescence associated with accumulation of p53 and $p16^{INK4a}$. Cell 88, 593–602.

Tan, Q., Huang, Q., Ma, Y., Mao, K., Yang, G., Luo, P., Jin, Y., 2018. Potential roles of IL-1

subfamily members in glycolysis in disease. Cytokine Growth Factor Rev. 44, 18–27.
The Burden of Musculoskeletal Diseases in the United States (BMUS), 2008. American Academy of Orthopaedic Surgeons. Retrieved from:. http://www.boneandjointburden.org/docs/TheBurdenofMusculoskeletalDiseasesintheUnitedStates(BMUS)1stEdition(2008).pdf.
Vo, N.V., Hartman, R., Yurube, T., Jacobs, L.J., Sowa, G.A., Kang, J., 2013. Expression and regulation of metalloproteinases and their inhibitors in intervertebral disc aging and degeneration. Spine J. 13 (3), 331–341.
Wang, C., Jurk, D., Maddick, M., Nelson, G., Martin-Ruiz, C., von Zglinicki, T., 2009. DNA damage response and cellular senescence in tissues of aging mice. Aging Cell 8 (3), 311–323.
Wang, Feng, Cai, Feng, Shi, Rui, Wang, Xiao-Hu, Wu, Xiao-Tao, 2015. Aging and Age Related Stresses: A Senescence Mechanism of Intervertebral Disc Degeneration. Retrieved October 14, 2015. Osteoarthritis and cartilage / OARS, Osteoarthritis Research Society. http://www.sciencedirect.com/science/article/pii/S1063458415013333.
Westermann, B., 2012. Bioenergetic role of mitochondrial fusion and fission. Biochim. Biophys. Acta 1817 (10), 1833–1838.
Wiley, C., Campisi, J., 2016. From ancient pathways to aging cells: connecting metabolism and cellular senescence. Cell Metab. 23 (6), 1013–1021.
Yang, H., Wang, H., Ren, J., Chen, Q., Chen, Z.J., 2017. cGAS is essential for cellular senescence. Proc. Natl. Acad. Sci. U. S. A. 114 (23), E4612–E4620.
Zhu, Y., Tchkonia, T., Pirtskhalava, T., Gower, A., Ding, H., Giorgadze, N., Kirkland, J.L., 2015. The Achilles' heel of senescent cells: from transcriptome to senolytic drugs. Aging Cell 14 (4), 644–658.